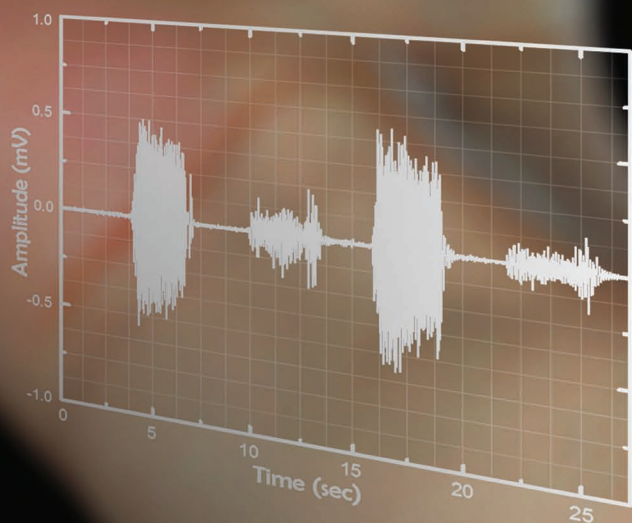


www.advmat.de

ADVANCED MATERIALS



Materials and Optimized Designs for Human-Machine Interfaces Via Epidermal Electronics

Jae-Woong Jeong, Woon-Hong Yeo, Aadeel Akhtar, James J. S. Norton, Young-Jin Kwack, Shuo Li, Sung-Young Jung, Yewang Su, Woosik Lee, Jing Xia, Huanyu Cheng, Yonggang Huang, Woon-Seop Choi, Timothy Bretl, and John A. Rogers*

Surface electromyography (sEMG) is a non-invasive technique for measuring electrical signals generated by the contraction of skeletal muscles. sEMG involves sensors placed on the skin, and can be exploited for many clinical and research purposes, ranging from diagnosing neuromuscular disorders,^[1] studying muscle pain,^[2,3] and controlling prosthetic or orthotic devices.^[4] In all instances, the measuring devices and, in particular, their interfaces to the skin must maximize signal levels while minimizing noise and crosstalk from non-targeted muscle groups. At the same time, form factors that enable soft, conformal adhesion, in ways that do not constrain the motions induced by muscle contractions, are essential for accurate measurement and long-term use without irritation or interface failure. Traditional sEMG signal measurements use rigid electrodes coupled to the skin via electrolyte gels, affixed with adhesive tapes or straps. Although valuable for uses in hospitals and other controlled settings, the ability to extend this type of technology to continuous monitoring in everyday life is frustrated

by discomfort associated with the electrodes, inconveniences that follow from bulk wired connections to external electronics, and reductions in measurement fidelity caused by drying of the gels. These same features also practically limit mounting locations to large, relatively flat regions of the body, such as the forehead, back, chest, forearm or thigh. The fingers, the face, the neck and other areas with sharp curvature, loose skin or high levels of tactile sensitivity cannot be addressed easily.

Recent research into new materials and mechanics designs demonstrates alternative means to integrate electrodes, and even fully integrated electronics and sensor systems, directly with the skin. These platforms exploit hybrid combinations of hard electrode materials with soft supports and matrix polymers to yield thin, mechanically compliant devices that can adopt the microscale topology of the skin, and can be mounted on nearly any region of the body. Examples include capacitive, biocompatible electrodes based on electrodes insulated with polydimethylsiloxane (PDMS)^[5] and skin adhesive patches that

Prof. J. A. Rogers
Department of Materials Science and Engineering
Beckman Institute for Advanced Science
and Technology, and Frederick Seitz Materials
Research Laboratory
University of Illinois at Urbana-Champaign
Urbana, Illinois, 61801, USA
E-mail: jrogers@illinois.edu

Dr. J.-W. Jeong,^[†] Dr. W.-H. Yeo,^[†] S. Li, W. Lee
Department of Materials Science and Engineering
Beckman Institute for Advanced Science and Technology
and Frederick Seitz Materials Research Laboratory
University of Illinois at Urbana-Champaign
Urbana, Illinois, 61801, USA

A. Akhtar
Medical Scholars Program, Neuroscience Program
University of Illinois at Urbana-Champaign
Urbana, Illinois, 61801, USA

J. J. S. Norton
Neuroscience Program
University of Illinois at Urbana-Champaign
Urbana, Illinois, 61801, USA

Prof. T. Bretl
Department of Aerospace Engineering
University of Illinois at Urbana-Champaign
Urbana, Illinois, 61801, USA

Y.-J. Kwack, Prof. W.-S. Choi
School of Display Engineering
Hoseo University
Asan, 336-795, Republic of Korea

S.-Y. Jung
Department of Mechanical engineering
Pohang University of Science and Technology
Pohang, 790-784, Republic of Korea

Y. Su
Center for Mechanics and Materials
Tsinghua University
Beijing 100084, China
Department of Civil and Environmental Engineering
Department of Mechanical Engineering
Center for Engineering and Health
Northwestern University
Evanston, Illinois, 60208, USA

J. Xia
Department of Engineering Mechanics
Tsinghua University
Beijing 100084, China
Department of Civil and Environmental Engineering
Department of Mechanical Engineering
Center for Engineering and Health
Northwestern University, Evanston
Illinois, 60208, USA

H. Cheng, Prof. Y. Huang
Department of Civil and Environmental Engineering
Department of Mechanical Engineering
Center for Engineering and Health Northwestern University
Evanston, Illinois, 60208, USA

^[†]These authors contributed equally to this work.



DOI: 10.1002/adma.201301921

use biomimetic micropillars.^[6,7] A class of technology referred to generically as epidermal electronic systems (EES)^[8] offers not only electrode interfaces to the skin but also integrated electronics for signal amplification and other functions. The materials and overall layouts of EES yield physical properties – area mass density, thickness and effective mechanical modulus – well matched to the epidermis itself. A consequence is that lamination directly onto the surface of the skin leads to intimate conformal contact, through the action of van der Waals adhesion alone. Details of this contact, and its impact on the electrical nature of the biotic/abiotic interface have not, however, been explored in detail. The following presents a series of systematic studies that summarize the key effects, and enable optimization of the performance of EES for sEMG. Examples include measurements obtained from wide ranging areas of the body and use of the resulting data for advanced forms of human-machine interface and control.

Measuring and accurately representing sEMG signals depend strongly on the design of the materials and structures of the sensors. Factors that determine the magnitude of electrical noise and crosstalk contamination include the electrode size, the inter-electrode distance, and the electrode shape and layout. For instance, the European concerted sEMG group has determined that electrodes with conventional designs should provide separations of 20 mm and dimensions of 10 mm, measured along the direction of the muscle fibers,^[9] for optimal results. Geometrical, material, and mechanical effects that influence the biotic/abiotic measurement interface of EES for sEMG are fundamentally different, in many respects. The essential issues are examined in detail in representative designs shown in **Figure 1a** and **1b**. Both the bar- and disk-type layouts incorporate narrow, thin interconnect wires, and gold electrodes (200 nm in thickness) in the form of filamentary serpentine (FS) meshes (Figure 1d) for measurement, ground, and reference. The interconnects use encapsulating layers of polyimide (PI; 300 nm in thickness, Sigma-Aldrich, USA) above and below to mitigate bending stresses in the metal; the traces terminate in exposed contact pads at one edge for the purpose of external connection and signal acquisition. The FS mesh electrodes involve bare metal on the bottom surfaces to enable direct electrical coupling to the skin. The layouts yield soft, elastic responses to applied strains, in a manner that both provides conformal contact to the skin and the ability to accommodate natural motions without mechanical constraint or interface delamination. FS traces with broad widths minimize contact impedance by providing large areal coverage, but such designs do not minimize principal strains associated with deformation. Increasing the radius of curvature of the FS can mitigate this disadvantage. An optimized combination of width (20 μm) and radius of curvature (45 μm) emerge from parametric studies using the finite element method (FEM) (see Supporting Information, Figure S1). Simulation and experimental results (Figure 1d and 1e) indicate that the resulting electrodes can be stretched over 30% with only 0.94% maximum principal strain in the metals (fracture strain of Au: 1%). This layout ensures robust operation at strain levels well beyond those that can be tolerated by the skin (10 – 20%).^[10] Such EES (see Experimental Section for fabrication process) can be integrated onto the skin by direct printing,^[11] or they can be delivered by use of

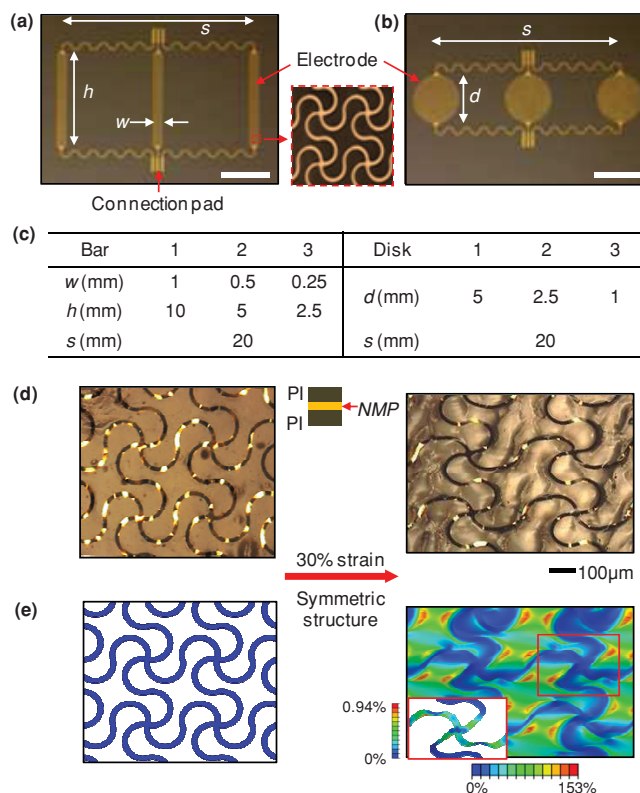


Figure 1. Designs and modeling results for epidermal electronic systems (EES) for surface electromyography (sEMG), including electrodes for measurement, ground and reference. (a) Image of bar-type designs, (b) Image of disk-type designs. The scale bar is 500 μm both for (a) and (b). The middle image shows a micrograph of the filamentary serpentine (FS) mesh structure used for the electrodes (width = 20 μm), (c) Table of design parameters. (d) Micrograph of a FS mesh structure before (left) and after (right) applying 30% strain. The inset in the middle illustrates the neutral mechanical plane (NMP) position of the metal layers (Au), with coatings of polyimide (PI) above and below. (e) FEM support of the experimental case in (d).

thin, low modulus silicone membrane substrates mounted on water-soluble polymer sheets (polyvinyl alcohol (PVA), Haining Sprutop Chemical Tech, China).^[11] This PVA sheet serves as a temporary support for manual lamination of the device on the skin, and is subsequently eliminated by applying water.^[8] The result is conformal integration of EES onto the skin, well configured for sEMG.

Studies of EES that have systematic variations in key parameters, including the membrane thickness, FS mesh electrode size, and inter-electrode separation, define the dependence of geometry, contact mechanics and layout on signal acquisition. Evaluations involve application of devices with different designs onto a given region of the flexor carpi radialis of the forearm of a single individual (Figure S2) after gently scrubbing the skin with a 70% isopropyl alcohol swab (Dukal, USA). The setup appears in Figure S2. Placing the forearm securely on a table and squeezing the hand to a well-defined bending force at the wrist (20N; Mark-10, USA) yields a reproducible, consistent level of muscle activity. Comparative analysis of different EES designs uses the average of sEMG signals measured during

three consecutive contractions, separated by 5 seconds of rest. An amplifier (TCP-128BA, James Long Company, NY) with built-in high-pass, low-pass, and notch filters and an acquisition system (IOtech Personal Daq 3000, Measurement Computing, MA; BCI 2000, National Instruments Data Acquisition Unit) serve as means to record sEMG data. The passband of the data acquisition electronics lies between 10–300 Hz. The low frequency cutoff eliminates any motion artifacts.

Conformal contact of the FS mesh electrodes with the skin is critically important to high fidelity measurement. The interface mechanics and soft adhesion at the biotic/abiotic interface determine the nature of this contact (Figures 2a and 2b). An analytical mechanics model in which the skin surface morphology is assumed to be sinusoidal with a characteristic amplitude (100 μm) and wavelength (140 μm) can capture the essential physics. Here, the critical membrane thickness below which van der Waals forces are sufficiently strong to drive perfect, conformal contact can be determined by considering the total energy associated with interfacial contact ($U_{\text{interface}}$) as [12]:

$$U_{\text{interface}} = U_{\text{EES_bending}} + U_{\text{skin_elasticity}} + U_{\text{adhesion}} \quad (1)$$

where $U_{\text{EES_bending}}$, $U_{\text{skin_elasticity}}$, and U_{adhesion} are the bending energy of the EES, the elastic energy of the skin, and the adhesion energy of the contact, respectively (see details of the analytical model in Supporting Information). The energy associated with localized deformations at the edges, which is typically negligible compared to that associated with bending, is not included in the analysis. The EES itself is treated as an effective composite material whose bending energy depends on the bending stiffness of both the EES electrodes (modulus of Au: 97 GPa, thickness including encapsulating PI layers: 800 nm, areal ratio of EES on the membrane: 33.7 %) and the membrane substrate (modulus of the membrane: 69 kPa; Ecoflex, Smooth-On, USA).^[11] The elastic energy of the skin is mainly determined by the wavelength (140 μm) and modulus (≈ 130 kPa) of the skin.^[13] Assuming that the contact adhesion is dominated by the interface between the EES, membrane, and the skin, the effective work of adhesion is ≈ 0.25 N m⁻¹.^[11]

Conformal contact results when the adhesion energy is larger than the sum of the bending and the elastic energy. Theoretical analysis (Figure 2b) shows that, for EES as in Figure 1, the critical membrane thickness is ≈ 25 μm . In other words, EES built using membranes with thicknesses smaller than this critical value will establish conformal contact to the skin. The analysis shows good qualitative agreement with experimental results (Figure 2a). In particular, a 5 μm -thick membrane makes excellent conformal contact with a polymer surface molded into the shape of human skin (forearm).^[11] At a thicknesses of 36 μm , air gaps can be observed at the interface; membranes with thicknesses of 100 μm and 500 μm show decreasing areas of contact, particularly at wrinkles and pits of the skin surface.

Conformal contact dictates not only the interface adhesion mechanics, but also the electrical contact impedance. This quantity, Z_c , can be expressed by [14]:

$$|Z_c| = \frac{\rho d}{A\sqrt{1 + (\omega\rho\varepsilon)^2}} \quad (2)$$

where ρ is the skin electrical resistivity, d is the inter-distance between electrodes, A is the contact area of the EES electrode with the skin, ω is signal source frequency, and ε is the skin dielectric constant. Measurements indicate that an increase in skin hydration, with other parameters fixed (i.e., A , d and ω), reduces Z_c (Figure 2c), consistent with an expectation that hydration level influences ρ and ε .^[15] In evaluating the effect of the EES thickness (5, 100, and 500 μm), measurements include separate determination of skin hydration level (hydration measurement by MoistureMeterSC Compact, Delfin Inc). Experimental determination of contact impedance involves measurements, using a built-in function of the amplifier (Model TCP-128BA, The James Long Company, NY) as in,^[14] before and after exfoliating the stratum corneum by repeated (three times) application and removal of ScotchTM tape. The results, summarized in Table 1, indicate a $\approx 30\%$ decrease in impedance on the flexor carpi radialis by removal of the stratum corneum. Even after accounting for variations in hydration level (between 19.6 and 20.7 for experiments reported here), the contact impedance increases systematically and significantly as the membrane thickness increases (Figure 2d). This result is consistent with expected trends in interfacial contact. The EES device that uses a 5 μm -thick membrane substrate shows remarkably low contact impedance, comparable to that of standard gel electrodes (5 μm -thick membrane EES: 24.4 k Ω @hydration = 19.6 vs. gel electrodes: 16.9 k Ω @hydration = 22.3). In addition to contact area, the impedance can depend on the choice of electrode materials.^[16] For realistic applications, an overriding consideration is in the use of biocompatible, non-corrosive, electrochemically stable materials that resist surface oxidation. In this sense, Au offers an attractive set of characteristics.

Conformal contact contributes to other aspects of improved performance, such as minimized motion artifacts and background noise. Figure 2e compares effects of the former in baseline signals obtained from an EES with a 5 μm -thick membrane and a separate conventional rigid sEMG electrode with coupling gel, located side by side. The ground electrode is shared, to facilitate direct comparison of these two systems. (For measurements of motion artifacts, the cutoff frequency of the high pass filter was set to 1 Hz.) Skin motions generated by applying periodic pressure to the skin at a localized region between the EES and the conventional electrode create parasitic features in the measured signals. Securing all external cabling and wires to the arm and table ensures that these features arise from the electrode themselves and their interfaces to the skin. (These features disappear when the electrodes are disconnected from the skin, in otherwise identical setups.) The results show that the EES interface provides signals that are minimally sensitive to skin deformation, by comparison to conventional electrodes. The differences likely arise from the ability of the EES construction to accommodate motions of the skin without relative motion of the electrodes and skin. By contrast, the gel in a conventional interface allows such motion, thereby creating slight time-dependent variations in the impedance and associated signals. Another benefit of EES follows from conformal contact to the skin. As shown in Figure 2f, the device with a 5 μm -thick membrane simultaneously offers the best skin contact and also achieves the smallest background noise (12 μV_{RMS}). Improved conformal contact results in increased levels of balance in impedance between the

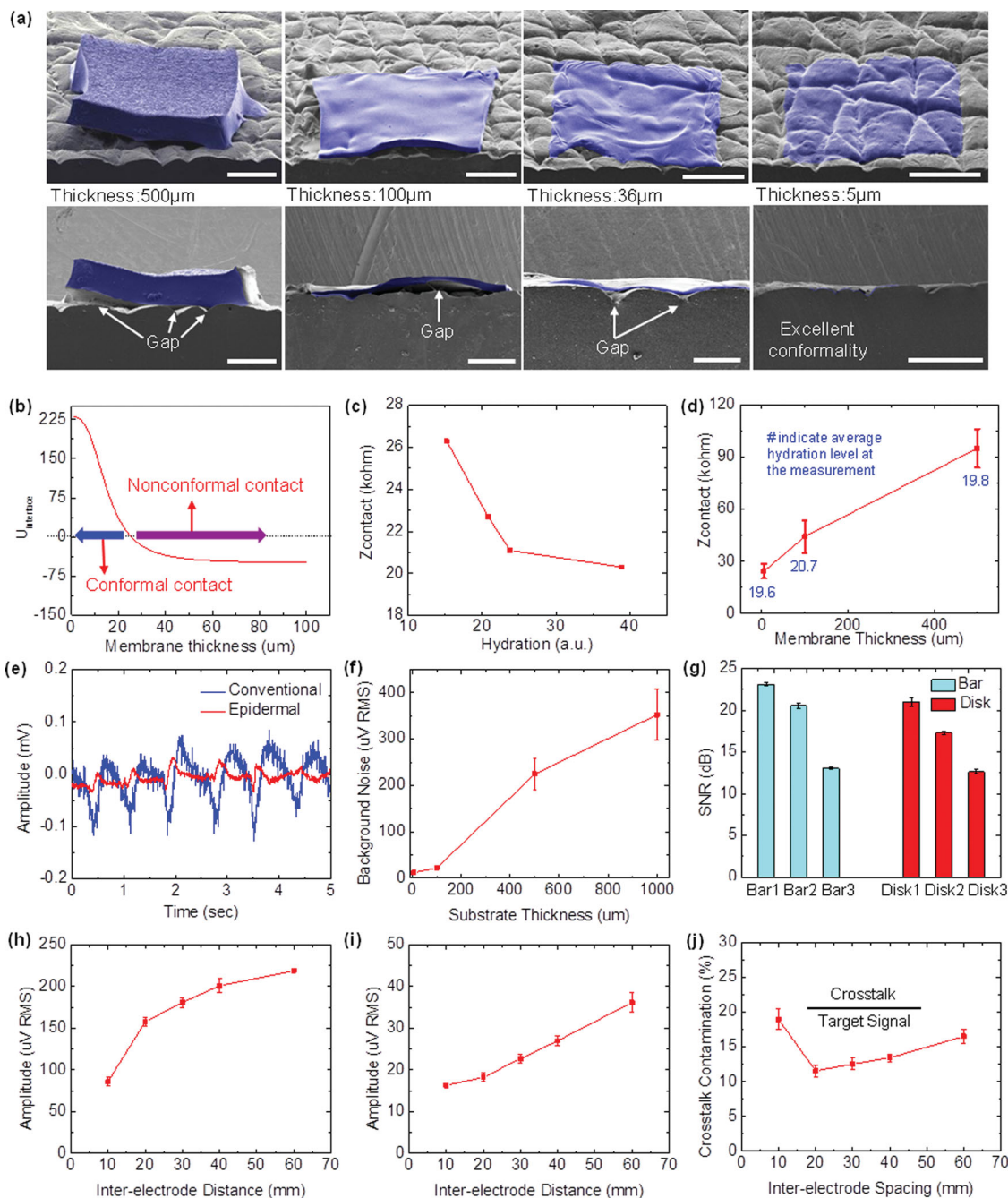


Figure 2. Colorized scanning electron microscope (SEM) images and measurement results obtained through systematic study of design choices in EES for sEMG. The relevant parameters include thickness of the supporting membrane, as well as electrode shape, size, and inter-electrode distance. (a) Angled and cross-sectional SEM images showing degree of conformal contact between a silicone replica of the surface of the skin (grey) and various thicknesses of elastomer membrane substrates (blue) for EES. (b) Analytical calculation of the energy associated with the interfacial contact ($U_{interface}$) between a representative skin surface and a membrane substrate as a function of thickness. Conformal contact occurs when $U_{interface} > 0$. (c) Contact impedance (Z_c) between EES electrodes and the skin, as a function of level of hydration in the skin, (d) Z_c as a function of thicknesses of the membrane substrate for an EES electrode, (e) Measured electrical signal (amplitude) as a function of time during mechanical deformation of the skin, for the case of EES (epidermal) and conventional rigid electrodes with gels, (f) Influence of the membrane substrate thickness on background noise of sEMG signals recorded with an EES. (g) Signal-to-noise ratio (SNR) for sEMG measured using EES with electrodes having different shapes and sizes. (h) Signal strength of sEMG measured from the flexor carpi radialis as a function of inter-electrode distance. (i) Crosstalk signal from the extensor muscle as a function of inter-electrode distance. (j) Crosstalk contamination as a function of the inter-electrode distance.

three electrode sites, which in turn leads to enhanced common mode rejection at the differential amplifier. Random variations in contact impedance associated with imperfect contacts using

thicker membranes cause increased noise amplitude and fluctuation (Figure S3). All of the following quantitative studies of FS electrode designs use EES with 5 μm -thick membranes.

Table 1. Contact impedance before and after exfoliation of stratum corneum.

Location	Impedance before Exfoliation (k Ω)	Impedance after Exfoliation (k Ω)	Impedance Decrease after Exfoliation (%)	Hydration Level
Right forearm at flexor carpi radialis	31.6	22.4	29.1	18.2
Right forearm near the wrist	29.5	21.2	28.1	20.6
Left forearm near the wrist	35.4	24.3	31.3	17.7

The electrical influence of geometry in bar- and the disk-type FS mesh electrodes can be determined by examining the signal-to-noise ratio (SNR) of sEMG signals measured using EES devices under controlled conditions. Following recommendations of the major standards body for bipolar sEMG electrodes,^[9] the inter-electrode distance is fixed at 20 mm for these studies. The Table in Figure 1c summarizes the design parameters, each of which corresponds to a variable shown in Figure 1a and 1b. As expected, upon an increase of the electrode size, the detected signal amplitudes and SNRs increase, due to an integrative effect on the sEMG signals (Figure 2g). The same consideration accounts for enhanced signals with disk-type electrodes, which have larger contact areas than corresponding bar-type designs with similar dimensions perpendicular to the muscle fibers. Among the different shapes and sizes, Bar1 exhibits the best SNR, due likely to an increased probability of signal detection that results from the large electrode size in the direction perpendicular to the muscle fibers.

The inter-electrode distance is a factor that influences both the signal amplitude and crosstalk. The latter is important because large signals from surrounding tissues can obscure measurements from targeted muscles. Studies involve the Bar1 design with various inter-electrode distances of 10, 20, 30, 40, and 60 mm. The magnitude of crosstalk is measured on the flexor carpi radialis from the extensor muscle during isometric contractions. Figures 2h and 2i show the mean and standard deviation of the RMS amplitude of the sEMG signals from the target (flexor carpi radialis) and crosstalk (extensor) muscles as a function of the inter-electrode distance. Although increasing this distance enhances both the signal amplitude and crosstalk, a ratiometric study of crosstalk and target muscle signal (Figure 2j) demonstrates that the smallest crosstalk contamination occurs at a spacing of 20 mm. Increases in crosstalk at larger distances arise from the greater spatial overlap of action potentials at the skin.^[17] Decreasing the electrode spacing from 20 mm to 10 mm increases the crosstalk contamination to the point that the crosstalk amplitude becomes comparable to that of the target signal. The collective results indicate, then, that the bar-type design with an electrode size of 10 mm \times 1 mm and an inter-electrode distance of 20 mm yields the best SNR with the smallest crosstalk in sEMG signals. This conclusion, which is consistent with findings obtained using conventional electrodes, applies only to measurements on the forearm flexor muscle. Other muscle groups require different dimensions. For example, the optimal design for conventional electrode interfaces to the *tibialis anterior* muscle with conventional electrodes involves 10 mm \times 1 mm bar type geometries with an inter-electrode distance of 10 mm.^[18]

The advanced materials and EES designs described above (Bar1) can be used to acquire high-quality sEMG signals on

nearly any region of the body. **Figure 3** shows examples of recordings obtained from the skin of the forearm, face, forehead, back of the neck and index finger. The first demonstration involves EES on both forearms (Figure 3a). The ground electrode, located in-between the measurement and reference electrodes (20 mm apart at center-to-center distance), determines the common-zero potential (Figure 3a). Although each bar-type electrode has an areal contact that is roughly half that of a corresponding gel-based conventional electrode used for comparison (Figure S4), the baseline noise levels are comparable (Figure S5). Signals obtained during bimanual gestures such as 'squeeze fists', 'bend wrists to the left', 'bend wrists to the right', and 'bend wrists outward' generate four characteristic sEMG patterns, as shown in Figure 3b. Figure 3c illustrates an example of EES configured for measuring sEMG signals on the face (muscle: *Masseter*), as an example of a location where conventional gel-based electrode might not be acceptable. Clenching the jaw and moving the mouth create different types of EMG signals, each of which is clearly distinguishable from the baseline noise (Figure 3d). Likewise, the EES on the forehead (targeted muscle: *Procerus*) and the back of the neck (targeted muscle: *Trapezius*) (Figures 3e and 3g) yield EMG signals associated with blinking and motions of the neck (Figures 3f and 3h), respectively. EES can even be wrapped onto the finger (Figure 3i; index finger, targeted muscle: *Vincula brevia*), where bending creates high-quality sEMG signals, in spite of the relatively small size of the corresponding muscle. The versatility in location demonstrated in these experiments suggests many possibilities in health, wellness monitoring, as well as in human-machine interface (HMI) technologies based on sEMG.

Measurement of sEMG signals on the forearms demonstrates the latter possibility through control of a drone quadrotor (AR. Drone, Parrot SA, Paris). The process flow for HMI in this case appears in Figure S6. Here, EES interfaces record sEMG signals from four different bimanual gestures (**Figure 4a**; EMG signals corresponds to the motions shown in the inset). Classification (see Experimental section for details) involves conversion of the raw data to root-mean-square (RMS) values according to

$$RMS = \sqrt{\frac{1}{N} \sum_{k=1}^N [x_k]^2} \quad (3)$$

where N is the number of samples and x_k is the k^{th} sample. These sEMG signals are binned into discrete commands using an linear discriminant analysis (LDA) classification algorithm. The accuracy of this classifier can then be visualized utilizing a confusion matrix (Figure 4b), in which the columns and rows represent the predicted class and the actual gestures

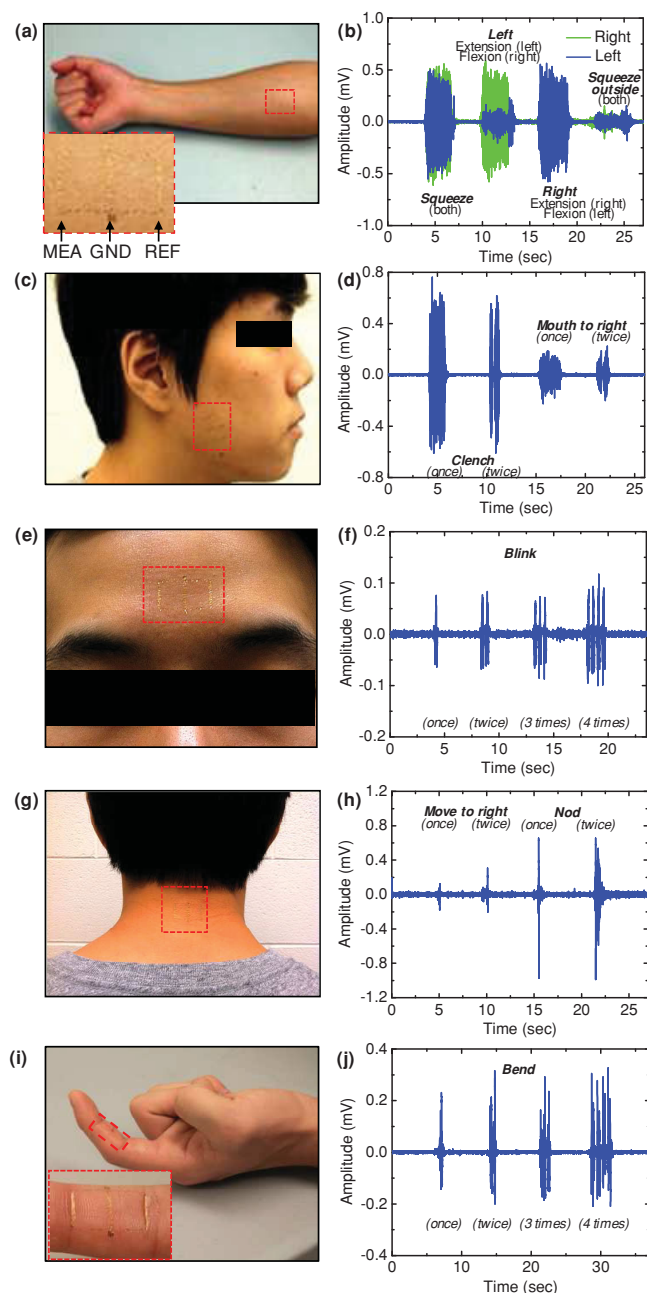


Figure 3. Applications of EES for sEMG signal sensing on various locations of the body. (a) EES on the forearm (target muscle: *Flexor carpi radialis*) including a magnified view of the device (inset) where MEA, GND, and REF refer to measurement, ground, and reference electrodes, respectively. (b) sEMG signals recorded from both forearms with four types of gestures. (c) EES on the face (target muscle: *Masseter*). (d) sEMG signals associated with clenching the jaw and moving the mouth. (e) EES on the forehead (target muscle: *Procerus*). (f) sEMG signals associated with blinking of the eyes. (g) EES on the back of the neck (target muscle: *Trapezius*). (h) sEMG signals associated with moving the neck. (i) EES on the index finger (target muscle: *Vincula brevia*). (j) sEMG signals associated while bending the finger.

(‘actual class’), respectively. As in the figure, the four gestures illustrated in Figure 4a correspond to distinct commands; In, Left, Right, and Out. As an example, the success rate for the

‘In’ command is 97.7 % for 43 trials. The overall accuracy of all four classifications is 91.1 %. The most significant confusion is observed for the ‘Out’ command, with 85.5 %. The accuracy can be improved with additional training and experience, enhanced classification algorithms, and the use of additional/different features in the data. The utility of this last strategy is demonstrated by enhanced classification accuracies observed in bimanual ($\approx 91\%$) compared to unimanual ($\approx 48\%$) gestures. The four gestures control the quadrotor for 5 different motions– 1st Out: ‘take off’, Right: ‘rotate clockwise’, In: ‘fly forward’, Left: ‘rotate counter-clockwise’, and 2nd Out: ‘land’ (Figure 4c; illustration is in top view). As demonstrated in Figure 4d, the flight of the quadrotor can be successfully controlled in this manner (Movie S1).

In conclusion, the studies reported here establish a set of guidelines in materials, mechanics and geometric designs for EES configured to measure sEMG signals. In optimized cases, the van der Waals interface between the EES and the skin yield robust and accurate measurement capabilities, with opportunities that lie outside those afforded by conventional electrode technologies. Many of the same general considerations apply to other measurement modalities, as well as to schemes for electrical and/or thermal stimulation.

Experimental Section

Fabrication of EES: Spin-coating polydimethylsiloxane (PDMS; 10 μm in thickness, Dow Corning, USA) on a glass slide followed by exposure to UV-ozone for 3 minutes creates a surface hydrophilic, for casting a layer of polyimide (PI; 300 nm in thickness through dilution with pyrrolidinone, Sigma-Aldrich, USA). Deposition and photolithographic patterning of Cr/Au (5nm/200nm in thickness) defines the electrode and interconnect structure. Encapsulating these features with a layer of PI (300nm in thickness) places the metal at the neutral mechanical plane. The final step involves exposing the EMG electrodes and pads for external connection by patterned reactive ion etching of corresponding regions of the top layer of PI.^[11] The result is a structure with a total thickness of 800 nm in an open, serpentine mesh design. A water-soluble tape (3M, USA) enables retrieval of the device from the PDMS-coated glass substrate and transfer to a thin silicone layer coated on a sheet of PVA. To establish strong bonds to the silicone, layers of Ti/SiO₂ (5nm/100nm) are deposited onto the contacting side of the device. The water-soluble tape is washed away after transferring the device to a silicone layer. Figure S7 (Supporting Information) demonstrates the process of transfer from the glass substrate to a membrane and subsequently to the skin.

Classification of EMG signals for HMI: The classification uses two channels of EMG data collected from each forearm, generated by contractions of the flexor carpi radialis. A 128-channel high impedance amplifier (Model TCP-128BA, The James Long Company, NY) yields analog data, converted to digital signals for analysis using MATLAB (The Mathworks, Inc., Natick, MA). To interact with the EMG control system, each participant performs four bimanual gestures: 1) squeeze fists, 2) bend wrists to the left, 3) bend wrists to the right, and 4) bend wrists outward. For training purposes, the participants perform each bimanual gesture five times for four seconds each. A baseline trial corresponds to the participant at rest for four seconds. Extraction and real-time classification uses a 250 ms sliding window with 100 ms overlap, to determine four features: root mean square (RMS), waveform length, zero crossings, and slope sign changes as describe elsewhere.^[19,20] A null state corresponds to an RMS value below 105% of the baseline. LDA^[20] serves to classify the features into discrete gestures. Following training, participants perform each gesture three times for three different

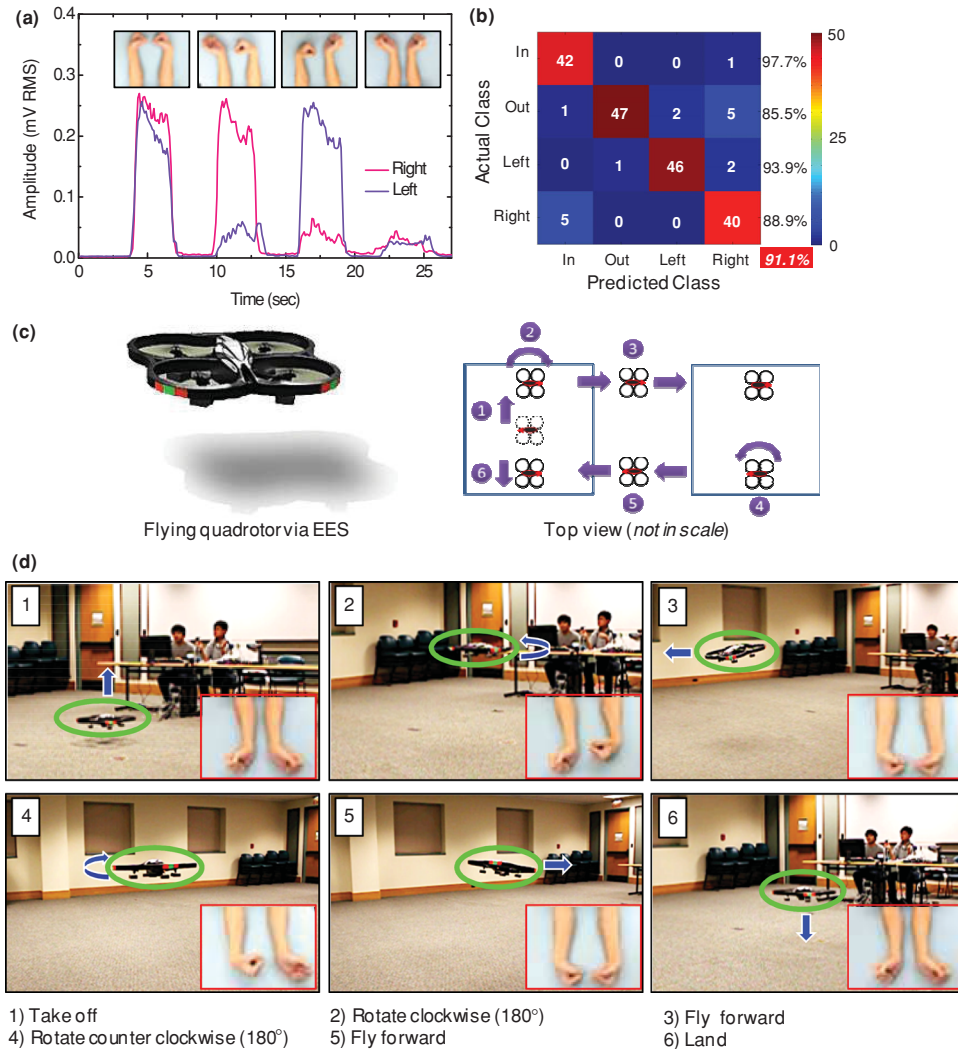


Figure 4. Human-machine interface (HMI) via sEMG signals recorded using EES. (a) sEMG signals recorded on forearms associated with four gestures. (b) Confusion matrix that describes the performance of the classification task; the number in the box and the color bar show the number of samples in the classification test. (c) Image of a remote operated quadrotor controlled via EES and the illustration of the control for 5 different motions (top view, not to scale). (d) Images of quadrotor control by sEMG signals from forearms. Insets show the control gestures.

durations (short, medium, and long). During this testing session, a conservative threshold minimizes other gesture classifications that occur during the null state. A priori examination of the training data determines this threshold.

Experiments on human subjects: All experiments were conducted under approval from Institutional Review Board at the University of Illinois at Urbana-Champaign (protocol number: 13229).

supported by the National Science Foundation under Grant DMI-0328162 and the US Department of Energy, Division of Materials Sciences under Award No. DE-FG02-07ER46471 through the Materials Research Laboratory and Center for Microanalysis of Materials (DE-FG02-07ER46453) at the University of Illinois at Urbana-Champaign. J.A.R. acknowledges a National Security Science and Engineering Faculty Fellowship.

Received: April 29, 2013

Published online: September 25, 2013

Supporting Information

Supporting Information is available from the Wiley Online Library or from the author.

Acknowledgements

J.-W.J. and W.-H.Y. contributed equally to this work. Authors appreciate the help of Jongwoo Lee with the schematic drawings. This study is

- [1] J. M. Gilchrist, G. M. Sachs, *Muscle Nerve* **2004**, *29*, 165.
- [2] C. Bodere, S. H. Tea, M. A. Giroux-Metges, A. Woda, *Pain* **2005**, *116*, 33.
- [3] D. Farina, L. Arendt-Nielsen, T. Graven-Nielsen, *Clin. Neurophysiol.* **2005**, *116*, 1558.
- [4] C. Castellini, P. Smagt, *Bio. Cyber.* **2009**, *100*, 35.
- [5] S. M. Lee, J. H. Kim, H. J. Byeon, Y. Y. Choi, K. S. Park, S.-H. Lee, *J. Neur. Eng.* **2013**, *10*, 1.

- [6] W. G. Bae, D. Kim, M. K. Kwak, L. Ha, S. M. Kang, K. Y. Suh, *Adv. Health. Mater.* **2013**, 2, 109.
- [7] M. K. Kwak, H.-E. Jeong, K. Y. Suh, *Adv. Mater.* **2011**, 23, 3949.
- [8] D.-H. Kim, N. Lu, R. Ma, Y.-S. Kim, R.-H. Kim, S. Wang, J. Wu, S. M. Won, H. Tao, A. Islam, K. J. Yu, T.-I. Kim, R. Chowdhury, M. Ying, L. Xu, M. Li, H.-J. Chung, H. Keum, M. McCormick, P. Liu, Y.-W. Zhang, F. G. Omenetto, Y. Huang, T. Coleman, J. A. Rogers, *Science* **2011**, 333, 838.
- [9] H. J. Hermens, B. Freriks, C. Disselhorst-Klug, G. Rau, *J. Electromyogr. Kinesiol.* **2000**, 10, 361.
- [10] N. Lu, C. Lu, S. Yang, J. A. Rogers, *Adv. Funct. Mater.* **2012**, 22, 4044.
- [11] W.-H. Yeo, Y.-S. Kim, J. Lee, A. Ameen, L. Shi, M. Li, S. Wang, R. Ma, S. H. Jin, Z. Kang, Y. Huang, J. A. Rogers, *Adv. Mater.* **2013**, 25, 2773.
- [12] S. Wang, M. Li, J. Wu, D.-H. Kim, N. Lu, Y. Su, Z. Kang, Y. Huang, J. A. Rogers, *J. Appl. Mech.* **2012**, 79, 031022.
- [13] H. Q. Jiang, Y. G. Sun, J. A. Rogers, Y. Huang, *Int. J. Solids Struct.* **2008**, 45, 2014.
- [14] L.-F. Wang, J.-Q. Liu, B. Yang, C.-S. Yang, *IEEE Sensors J.* **2012**, 12, 2898.
- [15] S. D. Campbell, K. K. Kraning, E. G. Schibli, S. T. Momn, *J. Investigat. Dermatol.* **1977**, 69, 290.
- [16] W. Besio, A. Prasad, presented at *EMBS Ann. Int. Conf.*, New York City, USA, Aug. 30 – Sept. 3, **2006**.
- [17] K. Roeleveld, D. F. Stegeman, H. M. Vingerhoets, A. Van Oosterom, *Acta Physiol. Scand.* **1997**, 160, 175.
- [18] C. J. De Luca, M. Kuznetsov, L. D. Gilmore, S. H. Roy, *J. Biomech.* **2012**, 45, 555.
- [19] J. Kim, S. Mastnik, E. André, presented at *the 13th int. conf. intelligent user interface*, **2008**.
- [20] T. A. Kuiken, G. Li, B. A. Lock, R. D. Lipschutz, L. A. Miller, K. A. Stubblefield, K. B. Englehart, *J. Am. Med. Assoc.* **2009**, 301.